# Accepted Manuscript


Super adsorption capability of rhombic dodecahedral Ca-Al layered double oxides for Congo red removal

Heng Zhang, Hang Chen, Seytkhan Azat, Zulkhair A. Mansurov, Xueming Liu, Jide Wang, Xintai Su, Ronglan Wu

PII: S0925-8388(18)32742-7

DOI: 10.1016/j.jallcom.2018.07.241

Reference: JALCOM 46957

To appear in: *Journal of Alloys and Compounds*

Received Date: 28 April 2018

Revised Date: 20 July 2018

Accepted Date: 21 July 2018

Please cite this article as: H. Zhang, H. Chen, S. Azat, Z.A. Mansurov, X. Liu, J. Wang, X. Su, R. Wu, Super adsorption capability of rhombic dodecahedral Ca-Al layered double oxides for Congo red removal, *Journal of Alloys and Compounds* (2018), doi: 10.1016/j.jallcom.2018.07.241.

**Graphical Abstract**

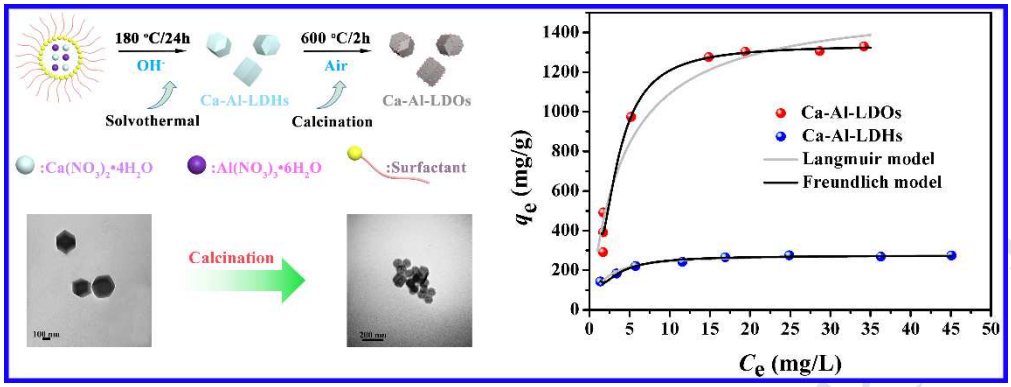

# Super adsorption capability of rhombic dodecahedral Ca-Al layered double oxides for Congo Red removal

Heng Zhang[a], Hang Chen[a], Seytkhan Azat[b], Zulkhair A. Mansurov [b], Xueming Liu[a], Jide Wang[a], Xintai Su[a]*, Ronglan Wu[a]*

[a]Ministry Key Laboratory of Oil and Gas Fine Chemicals, College of Chemistry and Chemical Engineering, Xinjiang University, Urumqi 830046, China

[b] Institute of Combustion Problems, Almaty 050012, Kazakhstan. Al-Farabi Kazakh National University, Almaty 050040, Kazakhstan

*Corresponding author: Xintai Su Tel. & fax: +869918581018. E-mail address: suxintai827@163.com.

*Corresponding author: Ronglan Wu. E-mail address: wuronglan@163.com.

**Abstract:**

In this work, a novel rhombic dodecahedral structure of Ca-Al-layered double hydroxides (Ca-Al-LDHs) was synthesized by a two-phase solvothermal method. Subsequently, Ca-Al layered double oxides (Ca-Al-LDOs) were obtained by calcinating Ca-Al-LDHs at 600 $^{o}$C which maintained the rhombic dodecahedral structures well. The morphologies of as-obtained samples were characterized by both transmission electron microscopy (TEM) and scanning electron microscopy (SEM). The phase structure and elemental composition were analyzed by X-ray diffraction (XRD) and energy dispersive X-ray spectroscopy (EDS)，respectively. Fourier transformed infrared (FT-IR) spectra were performed to confirm the existence of LDH structures. The Ca-Al-LDOs exhibited high adsorption rates and superb adsorption capacities for removal of Congo red (CR) from aqueous solution. The maximum adsorption capacities of Ca-Al-LDOs towards CR reached to 1536.1 mg·g$^{-1}$, which is extremely higher than most of hydrotalcite-like materials. The adsorption process of Ca-Al-LDHs and Ca-Al-LDOs were described by the Langmuir isotherm model and pseudo-second-order model well. The adsorption mechanisms mainly dominated by electrostatic adsorption, ion exchange process, hydrogen bonding interactions and surface complexation. This general strategy afforded a wide possibility to prepare a novel and advanced LDOs adsorption material for water treatment.

**Keywords:** Ca-Al layered double oxides; Congo red; Rhombic dodecahedral structure; Adsorption

## 1. Introduction

Organic contaminants in polluted water have become a serious environmental issue and received wide attention [1]. Among various organic pollutants, organic dyes are main pollutant source in water due to their wide applications in industries and uncontrolled emissions [2]. The direct discharge of wastewater containing organic dyes can lead to serious environmental pollution, intensify water crises and even harm human beings. Thus, diverse technologies have been developed to remove organic dyes such as adsorption [3], membrane filtration [4], photochemical degradation [5], flocculation [6], and ozonation techniques [7]. Among these methods, adsorption is a promising method because of its high efficiency, relatively low cost and simple operation [8]. A variety of adsorbents have been prepared to remove the dyes in wastewater such as carbon-based nano materials[9], graphene oxide[10], industrial waste[11], and polymer resins[12]. The selection and fabrication of adsorbents played a vital role in the adsorption technology. Generally, desirable adsorbents should be efficient, stable, low-cost, and environment-friendly. However, the low adsorption capability and recyclability of these adsorbents are main obstacles to apply them in water treatment. Hence, developing a new adsorbent with excellent adsorption capability, along with low production cost is currently still an important issue for basic research as well as practical applications.

The general formula of layered double hydroxides (LDHs) can be expressed by $[M_{1-x}^{2+}M_x^{3+}(OH)_2]^{x+}(A^{n-})_{x/n}\cdot mH_2O$), where $M^{2+}$ and $M^{3+}$ are divalent and trivalent metals respectively, and $A^{n-}$ represents the n-valent anion[13]. Furthermore, LDHs are also known as anionic clays, have been reported as a potential adsorbent for removing anionic pollutants from wastewater, which can be attributed to their layered structure, high porosity, and interlayer anion mobility of its $A^{n-}$ host[14]. In recent years, plenty of literature have reported application of binary LDHs on the adsorption of dyes and heavy metal ions, such as Ni-Fe-LDHs[15], Ni-Al-LDHs[16], and Mg-Fe-LDHs[17]. These LDHs with desirable morphologies have been widely researched, because of their fantastic porous structure and structural stability. Many researchers have tried to utilize calcined[18], intercalated[19] and modified[20] methods to further improve LDHs adsorption performance. Calcination treatment contributes to reduce the aggregation of LDHs and enhance the surface defects of materials. For example, Li et al.[21] have confirmed that calcination of polydopamine decorated Mg-Al-LDHs nanoflakes could greatly improve adsorption capacity of toxic metals and anionic dyes. The Mg-Ni-Al-LDOs derived from Mg-Ni-Al-LDHs prepared with a co-precipitation method have depicted a better adsorption performance for removal of methyl orange than the uncalcinated LDHs, which has been researched by Hassina's group[22].

Two-phase solvothermal method is a novel synthetic route to prepare some nanocrystals with special morphologies[23]. Some of the $Mg(OH)_2$ and AlOOH nanostructures and their derivatives with excellent adsorption properties synthesized with two-phase solvothermal method have been reported by our group[24, 25]. In this work, the novel rhombic dodecahedral Ca-Al-LDHs was fabricated by a two-phase solvothermal process. After calcination treatment, the rhombic dodecahedral Ca-Al layered double oxides (LDOs) were obtained. The Ca-Al-LDHs and Ca-Al-LDOs were used as adsorbents for adsorption of Congo red (CR)from aqueous solution to and compared its adsorption properties. Furthermore, the XRD and FT-IR techniques were investigated to evaluate the interaction mechanism

of CR with the Ca-Al-LDHs and Ca-Al-LDOs.

**2. Experimental section:**

**Materials**: All chemicals were of analytical grade and used as received without any further purification. Calcium nitrate tetrahydrate ($Ca(NO_3)_2 \cdot 4H_2O$, 99.0%) was purchased from Tianjin Yaohua Chemical Reagents Co., Ltd. Aluminium nitrate nonahydrate ($Al(NO_3)_3 \cdot 9H_2O$,99.0%) was purchased from Tianjin Hongyan Chemical Reagents Co., Ltd. Sodium hydroxide (NaOH,96.0%) was purchased from Tianjin Baishi Chemical Reagents Co., Ltd. Sodium oleate ($C_{18}H_{35}COONa$ or NaOA, 98%) was purchased from Tokyo Chemical Industry Co., Ltd. Absolute n-hexane and ethanol were purchased from Tianjin Baishi Chemical Reagents Co., Ltd. Thermostat oil bath was purchased from Jin Yi Instrument Co., Ltd., China. All the deionized water (with resistivity up to 18.2 MΩ/cm) was prepared by a UPC-III-40L pure Ultrapure Water System (China). The autoclave were purchased by Anhui Kemi Machinery Technology Co., LTD and the pressure of the autoclave was approximately 10.2 Mpa when the temperature reached 180 $^oC$.

**2.1 Preparation of Ca-Al-LDHs and Ca-Al-LDOs**

In a typical synthesis process, 2 mmol of $Ca(NO_3)_2 \cdot 4H_2O$ (0.472g), 1 mmol of $Al(NO_3)_3 \cdot 9H_2O$ (0.375 g) and 7 mmol of NaOA (2.132 g) were added to the solution containing 20 mL of absolute ethanol, and 30 mL of n-hexane. The mixed solution was stirred at 70 $^oC$ for 1 hour at about 600 rpm by using a thermostat oil bath (DF-II). Then 10ml of 0.7M sodium hydroxide aqueous solution was added and the mixture was stirred for 1 h. After cooled to room temperature, then sealed in a Teflon-lined stainless-steel autoclave (100 mL capacity) and heated at 180 °C for 24 h, the obtained white precipitate of Ca-Al-LDHs was washed and centrifuged in a TG-20G centrifuge (Kate laboratory equipment Co., Ltd, Yancheng, China) for 8 min at 10000 rpm with anhydrous alcohol and n-hexane three times, respectively. Finally, the washed Ca-Al-LDHs were dried at 60 $^oC$ for 12 h. The as-synthesized sample was heated at 600 $^oC$ for 2 h in a muffle furnace to obtain Ca-Al-LDOs. The synthesis of these materials is illustrated in Fig 1.

**2.2 Characterization of Ca-Al-LDHs and Ca-Al-LDOs**

The crystal structure of the as-synthesized products were determined by a Rigaku D/max-ga X-ray diffractometer (XRD) at a scanning rate of $6^o \cdot min^{-1}$using Cu Kα radiation (λ = 1.54178 Å) in 2θ ranging from $10^o$ to $80^o$. The morphologies and microstructures of the obtained particles were characterized with a transmission electron microscopy (TEM, HitachiH-600). The synthesized nanocrystals were observed with field-emission scanning electron microscope (FESEM) on a Hitachi SU-8000 field emission electron microscope operating at 20 kV. X-ray photoelectron spectroscopy (XPS) measurements were performed on a Thermo XPS ESCALAB 250Xi instrument with an Al $K_\alpha$ (1486.8 eV) X-ray source. The specific surface area and pore size distribution were obtained by the nitrogen adsorption–desorption isotherms and via the Brunauer–Emmett–Teller (BET) and Barrett-Joyner-Halenda (BJH) method. Nitrogen adsorption-desorption measurements were performed on a Micromeritics ASAP 2020 physisorption instrument at 77 K. Fourier Transform Infrared Spectrum (FT-IR) of the samples were taken in KBr pellets by using a Bruker EQUINOX-55 spectrometer (Bruker Optics Inc., Germany) within the range of 4000-400 $cm^{-1}$. The concentrations of CR in aqueous solutions were acquired with the use of a UV-vis spectrophotometer (UV-2450PC,

Shimadzu, Japan).

### 2.3 Adsorption experiment

Typically, the adsorption kinetic experiments were conducted by adding 20 mg adsorbent to 100 mL of 100 mg·$L^{-1}$ CR solution at natural pH (ca.7) under rate of stirring 800 rpm at room temperature (303 ± 2 K). At different time intervals, approximately 3 mL of aqueous solution were taken from the suspension, and the adsorbent were separated from the solution were centrifuged in a TGL-16C centrifuge (Shanghai Anting Instrument Factory, Shanghai, China) at 10000 rpm for 3 min . UV–vis adsorption spectra (UV- 2450PC) was used to analyze the concentration of CR remained in the upper clean solution at the maximum absorption wavelength of 490 nm. The adsorption capacity of the adsorbents at time t, $q_t$ (mg $g^{-1}$), was also calculated:

$$q_t = \frac{(C_0 - C_t)V}{m} \quad (1)$$

where $C_t$ is the concentration of CR at contact time $t$ (mg $L^{-1}$), $V$ (L) is the volume of the CR solution and $m$ (g) is the weight of adsorbents.

To evaluate the maximum adsorption capacity of the as-prepared material for CR, 2mg of as-prepared sample was added to a 10 ml of CR solutions with different concentration (30-300mg·$L^{-1}$) at natural pH (ca.7). The adsorption isotherm was obtained by varying the equilibrium CR concentrations $C_e$ (mg·$L^{-1}$) with stirring for 48 h at room temperature (303 ± 2 K). The amount of CR adsorbed on the sample at equilibrium $q_e$ (mg·$L^{-1}$) was calculated by using the following equation:

$$q_e = \frac{(C_0 - C_e)V}{m} \quad (2)$$

where $C_0$ (mg/L) is the initial CR concentration, $V$ (L) is the volume of the CR solution and $m$ (g) is the mass of the Ca-Al-LDHs or Ca-Al-LDOs.

The recyclability of the adsorbent was evaluated by repetition of adsorption/calcination cycles using the same Ca-Al-LDOs sample. A constant Ca-Al-LDOs dosage of 200 mg·$L^{-1}$ was placed in 100 mg·$L^{-1}$ CR solutions at room temperature (303 ± 2 K) and kept in contact for 12 h. The used Ca-Al-LDOs powder was calcined and reused in the same conditions. This procedure was repeated six times and the adsorption capacity was calculated for each cycle. All the experimental data were the average of triplicate determinations. The relative errors of the data were about 5%.

## 3. Result and discussion

### 3.1. Ca-Al-LDHs and Ca-Al-LDOs phase structure

The crystal phase of the as-synthesized Ca-Al-LDHs and Ca-Al-LDOs samples examined by XRD as presented in Fig 2,Twelve major diffraction peaks marked in blue color of the Ca-Al-LDHs sample are located at approximately 17.2$^o$, 19.9$^o$, 28.3$^o$, 31.8$^o$, 36.4$^o$, 39.2$^o$, 44.3$^o$, 52.4$^o$, 54.5$^o$,58.6$^o$, and 66.4$^o$. These peaks can be indexed to (211), (220), (321), (400), (420), (431), (521), (611),(640), (642), (800) and (840) planes of Katoite (JCPDS24-0217). After calcination at 600 $^o$C, the layered structure of Ca-Al-LDHs material was changed into bimetallic oxide Ca-Al-LDOs. The Ca-Al-LDOs sample exhibited nine diffraction peaks located at approximately at 17.8$^o$, 29.2$^o$, 33.1$^o$, 36.3$^o$, 40.9 $^o$, 46.2 $^o$, 54.8 $^o$, 57.1$^o$and 66.7$^o$that corresponded to the (211), (400),(420), (422), (521), (611), (640), (642) and (831) planes of Mayenite (JCPDS 48-1882). No other peaks were observed, indicating the high purity

of the obtained Ca-Al-LDHs and Ca-Al-LDOs.

### 3.2. Morphology and elemental composition

In order to characterize the microscopic architectures and composition of the as-obtained samples, SEM, TEM and EDS is employed. As shown in Fig 3 and 4,the pristine Ca-Al-LDHs sample appears to be rhombic dodecahedral morphology, which exhibited an average diameter of 150nm (Fig 3c and 4b). The surface of the rhombic dodecahedral Ca-Al-LDHs is smooth from different view angles. As for the Ca-Al-LDOs sample is with the same sizes (Fig 3f and 4d), shows a mixture of the nanoparticle and rhombic dodecahedron morphologies, with the nanoparticles attaching on the rhombic dodecahedron. The energy dispersive X-ray spectroscopy (EDS) spectrum of the Ca-Al-LDOs (Fig4h) exhibited the presence of Ca, Al, and O elements and the corresponding weight percentages are14.14%, 23.23%, and 62.63%, respectively. As displayed, Ca, Al, and O distribute homogeneously in the rhombic dodecahedral area. This result corroborates that Ca-Al double metal oxide were successfully obtained.

### 3.3. Nitrogen adsorption-desorption isotherms

To obtain the Ca-Al-LDHs and Ca-Al-LDOs specific surface area and pore structure distribution, $N_2$ adsorption-desorption analysis was conducted. Fig 5 displayed the Ca-Al-LDHs (Fig 5a) and Ca-Al-LDOs (Fig 5b) nitrogen adsorption–desorption isotherms and Barrett-Joyner-Halenda pore size distribution (inset). The results indicate that the as-prepared samples adsorption amount at a relative pressure approach 1.0 increased dramatically, because of the filling of spaces in Ca-Al-LDHs and Ca-Al-LDOs. The pore size distribution of the Ca-Al-LDHs and Ca-Al-LDOs emerged as unimodal porosity, owing to the macropores with pore diameters of 77.68 nm and 89.96nm, respectively. The $N_2$–BET surface area was 20.46 $m^2/g$ for Ca-Al-LDHs, and 17.30 $m^2/g$ for Ca-Al-LDOs. The Ca-Al-LDOs surface area is lower than Ca-Al-LDHs, which could be due to collapse of the sheets into large and dense aggregates upon calcination[26].

### 3.4. FTIR spectrum

Fourier transform infra red (FT-IR) spectra of Ca-Al-LDHs and Ca-Al-LDOs was performed and the results are shown in Fig 6. The large and broad band observed at 3438$cm^{-1}$and 3661 $cm^{-1}$can be attributed to O-H stretching vibration of interlayer water molecules and of OH groups[27, 28], and the weak band of Ca-Al-LDHs at ca. 3000 $cm^{-1}$is indication of the water molecules, which was attributed to the hydrogen-bond in the interlayer[29]. This weak band disappeared in Ca-Al-LDOs indicated that the interlayer anions were removed during the high temperature calcination process. The IR spectrum of Ca-Al-LDHs and Ca-Al-LDOs samples exhibits absorptions at 1428 and 1416 $cm^{-1}$ respectively, on account of the presence of intercalated $NO_3^-$ anions[27]. The bands of Ca-Al-LDOs at 828 $cm^{-1}$, and 567 $cm^{-1}$were attributing to metal-oxygen and metal-hydroxyl stretching[22, 30, 31].

### 3.5. XPS spectrum

The chemical composition and chemical status of the Ca-Al-LDOs were investigated using X-ray photoelectron spectroscopy (XPS). The survey spectrum (Fig7a) revealed the presence of Ca, Al, O, and C: these were the predominant elements in the Ca-Al-LDOs. In Fig. 7b, the XPS spectra of Al species present one dominant peak at approximately 73.3 eV, which is ascribed to Al $2p_{1/2}$ of $Al_2O_3$[32]. In Fig 7c, the double peak characteristic of Ca 2p at 346.3 eV and 349.8 eV are corresponding to Ca $2p_{3/2}$ and Ca $2p_{1/2}$, respectively[33]. The high-resolution XPS spectrum of O 1s is shown in Fig. 7d, the

two peaks at 530.3 and 531.5 eV corresponded to Ca−O, Al−O bonds[34]. The XPS analysis is consistent with the aforementioned EDS spectrum and powerful to demonstrate the bimetal mixed oxides in the Ca-Al-LDOs sample.

### 3.6. Adsorption kinetic and isotherm

Kinetic studies are essential for the evaluation of adsorption owing to this approach can describe the adsorption rate and elucidate the adsorption mechanism of sorption reactions.[35] The CR adsorption on Ca-Al-LDHs and Ca-Al-LDOs as an impact of contact time and room temperature are exhibited in Fig 8. One could see that the Ca-Al-LDOs sample shown two-stepped kinetic and the single kinetic was observed for Ca-Al-LDHs. The speed of CR adsorbed by both Ca-Al-LDHs and Ca-Al-LDOs increases rapidly in ~25 min. The CR adsorption on Ca-Al-LDHs reached equilibrium state around 80 min, and then sustained the adsorption capacity. Comparing to the adsorption of CR on Ca-Al-LDHs, the CR adsorption on Ca-Al-LDOs reached first equilibrium around 80 min, and then followed by a second increase of adsorbed CR, reaching a second plateau after 150 min. The first step was ascribed to the assimilate CR on the plenty and obtainable external surface adsorption sites. The second step on account of the adsorption of CR onto the inner surface adsorption sites, which are restricted by the internal particle diffusion mechanism.[36]

To explain the adsorption mechanism on the Ca-Al-LDHs and Ca-Al-LDOs samples, the kinetics of CR adsorption were analyzed by two kinetic models, including pseudo-first-order[37] and pseudo-second-order kinetics[38], which were expressed as follows:

$$\log\ (q_e - q_t) = \log\ q_e - K_1\, t/2.303 \quad (3)$$

$$t/\ q_t = 1/(\ K_2 q_e^{2}) + t/\ q_e \quad (4)$$

where $K_1$ ($min^{-1}$) and $K_2$ (g $mg^{-1}$ $min^{-1}$) are signified kinetic adsorption rate constants of pseudo-first-order and pseudo-second-order models, $q_e$ (mg/g) is the adsorption capacity at equilibrium and $q_t$ (mg/g) is the adsorption capacity at time $t$ (min), respectively. As shown in Fig 9a and b, the fitting curves of the $t/q_t$ versus t for adsorption of CR on the as-prepared samples display good linearity. From the calculated kinetic model constants (Table 1), it was apparent to notice that the Ca-Al-LDHs and Ca-Al-LDOs were better fitted by pseudo-second-order model than the pseudo-first-order model. It is worthy to note that the $K_{2,2}$ constant rate ($2.8 \times 10^{-5}$ g $mg^{-1}$ $min^{-1}$) for Ca-Al-LDOs is much lower than the $K_{2,1}$ rate ($1.5 \times 10^{-3}$). This finding is fully consistent with our interpretation of adsorption being limited by the intra particles diffusion.

The adsorption isotherms on Ca-Al-LDHs and Ca-Al-LDOs were performed to investigate the adsorption capacity of the samples at varying initial concentrations of CR solution. Fig 10. reveals the adsorption isotherms of CR on the obtained samples at room temperature. The Langmuir and Freundlich models were serve to analyze the experimental data. In general, the Langmuir model presumes that the adsorbed molecules are adhere to the adsorbent surface in a monolayer.The mathematical formula of the Langmuir isotherm could be represented as[39]:

$$C_e/q_e = 1/(K_L\, q_m) + C_e/q_m \quad (5)$$

where $C_e$ (mg/g) and $q_e$ (mg/g) are the equilibrium adsorption concentration and capacity, resprctively; $q_m$ (mg/g) is the theoretical maximum adsorption capacity, and $K_L$ (L/mg) is the equilibriumconstant of the Langmuir sorption.

The Freundlich isotherm used to describe theadsorption on heterogeneous surfaces. The Freundlich isotherm model equation could be expressed as[40]:

$$\ln q_e = \ln K_F + (1/n) \ln C_e \quad (6)$$

where $K_F$[(mg/g)·(L/mg)$^{1/n}$] and n are empirical Freundlich constants, $K_F$is an indicator of the adsorption capacity, and 1/n is the correspond to the adsorption intensity. Sips isotherm is a combined form of Langmuir and Freundlich expression. The model is expressed as:

$$q_e = K_s C_e^{n_s} / (1 + a_s C_e^{n_s}) \quad (7)$$

where $K_s$ (L/g) and $a_s$ (L/mmol) is the Sips isotherm parameter, and $n_s$ is the Sips parameter describe samples surface heterogeneity. The parameters calculated from the three models were summarized in Table 2. It can be seen that the adsorption isotherms of CR on Ca-Al-LDHs and Ca-Al-LDOs were well fitted by Langmuir model ($R^2$>0.986), which suggest that CR adsorption is in monolayer mode.[41]The $K_L$ parameter value aquired for Ca-Al-LDHs samples was higher than that aquired for Ca-Al-LDOs, which corresponding to the lower energy requirement for the process using the calcined sample. The Langmuir isothermal theoretical maximum adsorption capacity for Ca-Al-LDOs was approximately 5 times higher than that of the Ca-Al-LDHs sample: 1536.1 mg·g$^{-1}$ and 285.7 mg·g$^{-1}$ at room temperature. Interestingly, the surface area of Ca-Al-LDOs is lower than that of Ca-Al-LDHs (Fig. 4), while the higher adsorption capacity of Ca-Al-LDOs. Specific surface areas cannot be considered the key parameter in determining as sorption onto adsorbents. The increase of adsorption capacity of Ca-Al-LDOs could be attributed to the abundant metal−oxide bonds (Ca−O and Al−O) and “memory effect”, which could provide more adsorption sites for CR adsorption on Ca-Al-LDOs. Table 3 shows the adsorption capacity of the Ca-Al-LDOs sample compared with other adsorbents for CR removal.

### 3.7. Recyclability of the Ca-Al-LDOs

The good stability and good recyclability of adsorbents are a critical factor for the practical applications. Therefore, it is important to highlight that the initial properties of Ca-Al-LDOs sample used in the adsorption experiments were recovered after thermal treatment at 600 °C for 2 h under air flow. Under these conditions the adsorbed CR can be decompose, and the adsorbent is recycled. As shown in Fig 11, six cycles of the activity were measured for prepared Ca-Al-LDOs. After the first use, the adsorption capacity reached 99.84, 98.36, 98.40, 96.63, 96.22 and 93.44 % of the initial capacity. This small reduction in adsorption capacity indicates an important reuse property of the LDH memory effect. Other studies have also shown good recyclability for different LDH compounds and diverse anionic dye molecules.[42, 43]

### 3.8. Adsorption mechanism

The mechanisms of CR adsorption onto the obtained rhombic dodecahedral structure samples have been investigated using FT-IR. The FT-IR spectra analysis of Ca-Al-LDHs and Ca-Al-LDOs

before and after adsorption CR was presented in Fig 12(a). Obviously, it can be seen many new peaks appeared after CR adsorption on both Ca-Al-LDHs and Ca-Al-LDOs in the FT-IR spectra. The new band at 1050 and 1176 $cm^{-1}$on Ca-Al-LDOs with sorbed CR should be attributed to S–O and S=O vibrations of CR, which could conclude that the CR molecules were fastened on the functional group of Ca-Al-LDOs surfaces.[44, 45] The O-H peak of Ca-Al-LDHs shifted from 3661 to 3482 $cm^{-1}$ after CR adsorption, which indicates that hydrogen bond formed by surface O-H of Ca-Al-LDHs might participate in adsorption process.[46] The O-H peak of Ca-Al-LDOs had no clear change after CR adsorption, suggesting that hydrogen bonding did not participate in CR adsorption on Ca-Al-LDOs. It is clear to see that the peaks of Ca-Al-LDHs and Ca-Al-LDOs have obvious change after CR adsorption at 450–900 $cm^{-1}$. The peaks of metal-oxygen-metal and oxygen-metal-oxygen stretching were disappeared or shifted after adsorption, suggesting that the metal ions ($Ca^{2+}$ and $Al^{3+}$) were complexed with single and double sulfur (S–O and S=O) of CR on the functional group of Ca-Al-LDHs and Ca-Al-LDOs groups.[47] This phenomenon shows that CR adsorption on Ca-Al-LDHs and Ca-Al-LDOs might be attributed to surface complexation, ion exchange between the metal ions and dye anions.

Fig 12(b) shows the XRD patterns of Ca-Al-LDHs and Ca-Al-LDOs adsorbents, meanwhile the Ca-Al-LDHs and Ca-Al-LDOs samples after adsorption of CR showed that many peaks disappeared. The XRD patterns of the adsorbents adsorption of CR have an evidence of crystalline state of adsorbents changing into amorphous state after adsorption, which suggests that the dye molecules diffuse into micropores and macropores of adsorbents. So one can conclude that adsorption of CR on Ca-Al-LDHs and Ca-Al-LDOs is mostly by chemisorption, which alter the structure of the layer space.[48, 57]

In addition, it can be concluded that the CR adsorption mechanism on Ca-Al-LDHs and Ca-Al-LDOs may be attributed to hydrogen bonding with oxygen or nitrogen, ion exchange and surface complexation. Furthermore, the Ca-Al-LDOs have a 3D hierarchically porous superstructure with nanoparticles, which may have facilitated rapid diffusion of CR molecules by serving as molecule-transport pathways, resulting in high adsorption of CR.

**4. CONCLUSION**

In summary, the Ca-Al-LDHs and Ca-Al-LDOs rhombic dodecahedral structures were prepared using facile synthetic methods and these samples have been studied as adsorbents for highly efficient

uptake of CR. The Ca-Al-LDOs sample could be better fits with Langmuir isotherm model and the maximum adsorption capacity for CR was 1536.1 mg $g^{-1}$, which was significantly higher than Ca-Al-LDHs. The adsorption kinetics of Ca-Al-LDHs and Ca-Al-LDOs were both demonstrated to well follow the pseudo-second-order model. The adsorption of CR on Ca-Al-LDHs and Ca-Al-LDOs may be mainly attributed to hydrogen bonding with oxygen or nitrogen, ion exchange and surface complexation. From the excellent adsorption capacity, the Ca-Al-LDOs can be serving as a kind of effective broad adsorbent for organic dyes as well as heavy metal ions, with a considerable application potential in wastewater treatment.

**Ackowledgments**

This work was supported by the National Natural Science Foundation of China (U1503391 and 21566037).

**References**

[1] Y. Cheng, F. Yan, F. Huang, W. Chu, D. Pan, Z. Chen, J. Zheng, M. Yu, Z. Lin, Z. Wu, Bioremediation of Cr(VI) and immobilization as Cr(III) by Ochrobactrum anthropi, Environmental Science & Technology, 44 (2010) 6357-6363.

[2] Z. Zhuang, H. Chen, Z. Lin, Z. Dang, $Mn_2O_3$ hollow spheres synthesized based on an ion-exchange strategy from amorphous calcium carbonate for highly efficient trace-level uranyl extraction, Environmental Science Nano, 3 (2016) 1254-1258.

[3] M. Chen, P. Wu, L. Yu, S. Liu, B. Ruan, H. Hu, N. Zhu, Z. Lin, FeOOH-loaded $MnO_2$ nano-composite: An efficient emergency material for thallium pollution incident, Journal of Environmental Management, 192 (2017) 31-38.

[4] M. Soylak, Y.E. Unsal, N. Kizil, A. Aydin, Utilization of membrane filtration for preconcentration and determination of Cu(II) and Pb(II) in food, water and geological samples by atomic absorption spectrometry, Food & Chemical Toxicology An International Journal Published for the British Industrial Biological Research Association, 48 (2010) 517-521.

[5] L. Qi, J. Yu, M. Jaroniec, Enhanced and suppressed effects of ionic liquid on the photocatalytic activity of TiO 2, Adsorption-journal of the International Adsorption Society, 19 (2013) 557-561.

[6] J.W. Lee, S.P. Choi, R. Thiruvenkatachari, W.G. Shim, H. Moon, Submerged microfiltration membrane coupled with alum coagulation/powdered activated carbon adsorption for complete decolorization of reactive dyes, Water Research, 40 (2006) 435-444.

[7] H. Selcuk, Decolorization and detoxification of textile wastewater by ozonation and coagulation processes, Dyes & Pigments, 64 (2005) 217-222.

[8] M. Liu, Y. Wang, L. Chen, Y. Zhang, Z. Lin, $Mg(OH)_2$ Supported Nanoscale Zero Valent Iron Enhancing the Removal of Pb(II) from Aqueous Solution, Acs Appl Mater Inter, 7 (2015) 7961-7969.

[9] M. Ji, X. Su, Y. Zhao, W. Qi, Y. Wang, G. Chen, Z. Zhang, Effective adsorption of Cr(VI) on mesoporous Fe-functionalized Akadama clay: Optimization, selectivity, and mechanism, Applied Surface Science, 344 (2015) 128-136.

[10] C. Zhao, L. Ma, J. You, F. Qu, R.D. Priestley, EDTA- and amine-functionalized graphene oxide as

sorbents for Ni(II) removal, Desalination & Water Treatment, 57 (2016) 1-10.
[11] H. Chen, J. Luo, X. Wang, X. Liang, Y. Zhao, C. Yang, M.I. Baikenov, X. Su, Synthesis of $Al_2O_3$ /carbon composites from wastewater as superior adsorbents for Pb(II) and Cd(II) removal, Microporous & Mesoporous Materials, 255 (2018) 69-75.
[12] M.A. Behnajady, S. Bimeghdar, Synthesis of mesoporous NiO nanoparticles and their application in the adsorption of Cr(VI), Chemical Engineering Journal, 239 (2014) 105-113.
[13] L.G. Yan, K. Yang, R.R. Shan, T. Yan, J. Wei, S.J. Yu, H.Q. Yu, B. Du, Kinetic, isotherm and thermodynamic investigations of phosphate adsorption onto core-shell $Fe_3O_4$@LDHs composites with easy magnetic separation assistance, Journal of Colloid & Interface Science, 448 (2015) 508-516.
[14] K.H. Goh, T.T. Lim, Z. Dong, Application of layered double hydroxides for removal of oxyanions: a review, Water Research, 42 (2008) 1343-1368.
[15] K. Nejati, Z. Rezvani, M. Mansurfar, A. Mirzaee, M. Mahkam, Adsorption of Metanil Yellow Azoic Dye from Aqueous Solution onto Mg–Fe–$NO_3$ Layered Double Hydroxide, Zeitschrift Für Anorganische Und Allgemeine Chemie, 637 (2011) 1573–1579.
[16] F.B. Saiah, B.L. Su, N. Bettahar, Nickel-iron layered double hydroxide (LDH): textural properties upon hydrothermal treatments and application on dye sorption, Journal of Hazardous Materials, 165 (2009) 206-217.
[17] C. Zhang, S. Yang, H. Chen, H. He, C. Sun, Adsorption behavior and mechanism of reactive brilliant red X-3B in aqueous solution over three kinds of hydrotalcite-like LDHs, Applied Surface Science, 301 (2014) 329-337.
[18] X. Wu, X. Tan, S. Yang, T. Wen, H. Guo, X. Wang, A. Xu, Coexistence of adsorption and coagulation processes of both arsenate and NOM from contaminated groundwater by nanocrystallined Mg/Al layered double hydroxides, Water Research, 47 (2013) 4159-4168.
[19] Y. Tian, G. Wang, F. Li, D.G. Evans, Synthesis and thermo-optical stability of o-methyl red-intercalated Ni–Fe layered double hydroxide material, Materials Letters, 61 (2007) 1662-1666.
[20] X. Ruan, Y. Chen, H. Chen, G. Qian, R.L. Frost, Sorption behavior of methyl orange from aqueous solution on organic matter and reduced graphene oxides modified Ni–Cr layered double hydroxides, Chemical Engineering Journal, 297 (2016) 295-303.
[21] X.K. Wang, J. Li, Q. Fan, C. Chen, Z. Tang, X. Wang, Y. Wu, Magnetic polydopamine decorated with Mg-Al LDH nanoflakes as a novel bio-based adsorbent for simultaneous removal of potentially toxic metals and anionic dyes, Journal of Materials Chemistry A, 4 (2016) 1737-1746.
[22] H. Zaghouane-Boudiaf, M. Boutahala, L. Arab, Removal of methyl orange from aqueous solution by uncalcined and calcined MgNiAl layered double hydroxides (LDHs), Chemical Engineering Journal, 187 (2012) 142-149.
[23] Y. Li, C. Yang, J. Ge, C. Sun, J. Wang, X. Su, A general microwave-assisted two-phase strategy for nanocrystals synthesis, Journal of Colloid & Interface Science, 407 (2013) 296-301.
[24] X. Liu, C. Niu, X. Zhen, J. Wang, X. Su, Novel approach for synthesis of boehmite nanostructures and their conversion to aluminum oxide nanostructures for remove Congo red, Journal of Colloid & Interface Science, 452 (2015) 116-125.
[25] X. Liu, C. Niu, X. Zhen, J. Wang, X. Su, Novel approach for the synthesis of $Mg(OH)_2$ nanosheets and lamellar MgO nanostructures and their ultra-high adsorption capacity for Congo red, Journal of Materials Research, 30 (2015) 1639-1647.
[26] R.L. Whitby, V.M. Gun'Ko, A. Korobeinyk, R. Busquets, A.B. Cundy, K. László, J. Skubiszewskazięba, R. Leboda, E. Tombácz, I.Y. Toth, Driving Forces of Conformational Changes in

Single-Layer Graphene Oxide, Acs Nano, 6 (2012) 3967-3973.
[27] A. Wongariyakawee, J.H. Warner, D. O'Hare, Surfactant directed synthesis of calcium aluminum layered double hydroxides nanoplatelets, Journal of Materials Chemistry, 22 (2012) 7751-7756.
[28] G. Carja, R. Nakamura, T. Aida, H. Niiyama, Textural properties of layered double hydroxides: effect of magnesium substitution by copper or iron, Microporous & Mesoporous Materials, 47 (2001) 275-284.
[29] Z.L. Hsieh, M.C. Lin, J.Y. Uan, Rapid direct growth of Li–Al layered double hydroxide (LDH) film on glass, silicon wafer and carbon cloth and characterization of LDH film on substrates, Journal of Materials Chemistry, 21 (2011) 1880-1889.
[30] S. Duan, J.X. Li, X. Liu, Y. Wang, S. Zeng, D. Shao, T. Hayat, HF-free synthesis of nanoscale metal–organic framework NMIL-100(Fe) as an efficient dye adsorbent, Acs Sustainable Chemistry & Engineering, 4 (2016) 3368-3378.
[31] J. Wang, X. Wang, L. Tan, Y. Chen, T. Hayat, J. Hu, A. Alsaedi, B. Ahmad, W. Guo, X. Wang, Performances and mechanisms of Mg/Al and Ca/Al layered double hydroxides for graphene oxide removal from aqueous solution, Chemical Engineering Journal, 297 (2016) 106-115.
[32] I.V. Plyuto, A.P. Shpak, S. Jerzy, L.F. Shara, Y.V. Plyuto, I.V. Babich, M. Michiel, J.A. Moulijn, XPS characterisation of carbon‐coated alumina support, Surface & Interface Analysis, 38 (2010) 917-921.
[33] P. Ghods, O.B. Isgor, J.R. Brown, F. Bensebaa, D. Kingston, XPS depth profiling study on the passive oxide film of carbon steel in saturated calcium hydroxide solution and the effect of chloride on the film properties, Applied Surface Science, 257 (2011) 4669-4677.
[34] H. Falcón, J.A. Barbero, G. Araujo, M.T. Casais, M.J. MartíNez-Lope, J.A. Alonso, J.L.G. Fierro, Double perovskite oxides A 2 $FeMoO_{6-\delta}$ (A=Ca, Sr and Ba) as catalysts for methane combustion, Applied Catalysis B Environmental, 53 (2004) 37-45.
[35] R. Chen, J. Yu, W. Xiao, Hierarchically porous $MnO_2$ microspheres with enhanced adsorption performance, Journal of Materials Chemistry A, 1 (2013) 11682-11690.
[36] Y.X. Zhang, X.D. Hao, T. Wang, Y.X. Meng, X. Han, MnO(x)-modified ZnAl-LDOs as high-performance adsorbent for the removal of methyl orange, Dalton Transactions, 43 (2014) 6667-6676.
[37] E. Demirbas, N. Dizge, M.T. Sulak, Adsorption kinetics and equilibrium of copper from aqueous solutions using hazelnut shell activated carbon, Chemical Engineering Journal, 148 (2009) 480-487.
[38] Y.S. Ho, G. Mckay, Pseudo-second order model for sorption processes, Process Biochemistry, 34 (1999) 451-465.
[39] I. Langmuir, The Adsorption of gas on plane surfaces of glass, mica and platinum, Journal of Chemical Physics, 40 (1918) 1361-1403.
[40] M. Ahmaruzzaman, S.L. Gayatri, Batch adsorption of 4-nitrophenol by acid activated jute stick char: Equilibrium, kinetic and thermodynamic studies, Chemical Engineering Journal, 158 (2010) 173-180.
[41] H. Chen, X. Wang, J. Li, X. Wang, Cotton derived carbonaceous aerogels for the efficient removal of organic pollutants and heavy metal ions, Journal of Materials Chemistry A, 3 (2015) 6073-6081.
[42] M.A. Ulibarri, I. Pavlovic, C. Barriga, M.C. HermosíN, J. Cornejo, Adsorption of anionic species on hydrotalcite-like compounds: effect of interlayer anion and crystallinity, Applied Clay Science, 18 (2001) 17-27.
[43] R.M.M.D. Santos, V.R.L. Constantino, C.V. Santilli, P.D. Borges, J. Tronto, F.G. Pinto,

Adsorption of Acid Yellow 42 dye on calcined layered double hydroxide: Effect of time, concentration, pH and temperature, Applied Clay Science, 140 (2017) 132-139.

[44] X. Mo, Z.H. Yang, H.Y. Xu, G.M. Zeng, J. Huang, X. Yang, P.P. Song, L.K. Wang, Combination of cathodic reduction with adsorption for accelerated removal of Cr(VI) through reticulated vitreous carbon electrodes modified with sulfuric acid-glycine co-doped polyaniline, Journal of Hazardous Materials, 286 (2015) 493-502.

[45] J. Wang, K. Zhang, L. Zhao, Sono-assisted synthesis of nanostructured polyaniline for adsorption of aqueous Cr(VI): Effect of protonic acids, Chemical Engineering Journal, 239 (2014) 123-131.

[46] Z. Jin, X. Wang, Y. Sun, Y. Ai, X. Wang, Adsorption of 4-n-Nonylphenol and Bisphenol-A on Magnetic Reduced Graphene Oxides: A Combined Experimental and Theoretical Studies, Environmental Science & Technology, 49 (2015) 9168-9175.

[47] J. Wang, D. Kang, X. Yu, M. Ge, Y. Chen, Synthesis and characterization of Mg–Fe–La trimetal composite as an adsorbent for fluoride removal, Chemical Engineering Journal, 264 (2015) 506-513.

[48] C. Namasivayam, D. Kavitha, IR, XRD and SEM studies on the mechanism of adsorption of dyes and phenols by coir pith carbon from aqueous phase, Microchemical Journal, 82 (2006) 43-48.

[49] Bai, Peng, Fabing Su, Pingping Wu, Likui Wang, F. Yin Lee, L. Lv, Zifeng Yan, And, X.S.Z., Copolymer-Controlled Homogeneous Precipitation for the Synthesis of Porous Microfibers of Alumina, Langmuir the Acs Journal of Surfaces & Colloids, 23 (2007) 4599-4605.

[50] X. Liu, C. Niu, X. Zhen, J. Wang, X. Su, Novel approach for synthesis of boehmite nanostructures and their conversion to aluminum oxide nanostructures for remove Congo red, Journal of Colloid & Interface Science, 452 (2015) 116-125.

[51] M. Szlachta, P. Wójtowicz, Adsorption of methylene blue and Congo red from aqueous solution by activated carbon and carbon nanotubes, Water Science & Technology A Journal of the International Association on Water Pollution Research, 68 (2013) 2240-2248.

[52] J. Hu, Z. Song, L. Chen, H. Yang, J. Li, R. Richards, Adsorption Properties of MgO(111) Nanoplates for the Dye Pollutants from Wastewater, Journal of Chemical & Engineering Data, 55 (2010) 3742-3748.

[53] L. Lian, L.P. Guo, A.X. Wang, Use of CaCl2 modified bentonite for removal of Congo red dye from aqueous solutions, Desalination, 249 (2009) 797-801.

[54] T. Hao, C. Yang, X. Rao, J. Wang, C. Niu, X. Su, Facile additive-free synthesis of iron oxide nanoparticles for efficient adsorptive removal of Congo red and Cr(VI), Applied Surface Science, 292 (2014) 174-180.

[55] I.M. Ahmed, M.S. Gasser, Adsorption study of anionic reactive dye from aqueous solution to Mg–Fe–CO3 layered double hydroxide (LDH), Applied Surface Science, 259 (2012) 650-656.

[56] B. Li, Y. Zhang, X. Zhou, Z. Liu, Q. Liu, X. Li, Different dye removal mechanisms between monodispersed and uniform hexagonal thin plate-like MgAl–$CO_3^{2-}$-LDH and its calcined product in efficient removal of Congo red from water, Journal of Alloys & Compounds, 673 (2016) 265-271.

[57] Lei C, Zhu X, Zhu B, et al. Superb adsorption capacity of hierarchical calcined Ni/Mg/Al layered double hydroxides for Congo red and Cr(VI) ions, Journal of Hazardous Materials, 321 (2017) 801-811.

**Table1.** Pseudo-first-order and pseudo-second-order kinetic model parameters of the as-obtained samples.

| Samples | Pseudo-first-order model | | | | | | Pseudo-second-order model | | | | | |
|---|---|---|---|---|---|---|---|---|---|---|---|---|
| | $q_{e1}$ (mg/g) | $q_{e2}$ (mg/g) | $K_{1,1}$ ($min^{-1}$) | $K_{1,2}$ ($min^{-1}$) | $R_1^2$ | $R_2^2$ | $q_{e1}$ (mg/g) | $q_{e2}$ (mg/g) | $K_{2,1}$ ($g\cdot mg^{-1}\cdot min^{-1}$) | $K_{2,2}$ ($g\cdot mg^{-1}\cdot min^{-1}$) | $R_1^2$ | $R_2^2$ |
| Ca-Al-LDHs | 203.7 | - | 0.01152 | - | 0.944 | - | 250 | - | $0.023\times10^{-3}$ | - | 0.997 | - |
| Ca-Al-LDOs | 228.6 | 498 | $2.4\times10^{-4}$ | $2.7\times10^{-4}$ | 0.915 | 0.779 | 229.4 | 613.5 | $1.5\times10^{-3}$ | $2.8\times10^{-5}$ | 0.997 | 0.968 |

**Table 2.** Adsorption isotherm parameters of the Ca-Al-LDHs and Ca-Al-LDOs samples.

| | Langmuir model | | | Freundlich model | | | Sips model | | |
|---|---|---|---|---|---|---|---|---|---|
| | $Q_{max}$ (mg/g) | $K_L$ (L/mg) | $R^2$ | $K_F$ ($mg^{1-n}$/g) | $n$ | $R^2$ | $K_s$ (L/g) | $n_s$ | $R^2$ |
| Ca-Al-LDHs | 285.7 | 0.65 | 0.999 | 146.9 | 5.43 | 0.980 | 95.6 | 1.55 | 0.943 |
| Ca-Al-LDOs | 1536.1 | 0.22 | 0.986 | 327 | 2.27 | 0.981 | 222.8 | 1.69 | 0.982 |

**Table 3.** Comparison of the adsorption CR on Ca-Al-LDOs sample and previously reported materials.

| Adsorbents | Adsorbates | $q_{max}$ (mg/g) | References |
|---|---|---|---|
| Ca-Al layered double oxides | CR | 1536.1 | this study |
| Ca-bentonite | CR | 107.4 | [49] |
| γ-$Al_2O_3$ nanorods | CR | 416.7 | [50] |
| Activated carbon powder | CR | 500 | [51] |
| MgO (111) nanoplates | CR | 303 | [52] |
| Mg/Al LDH nanoflakes | CR | 585 | [21] |
| Hierarchical NiO nanosheets | CR | 151.7 | [53] |
| α–$Fe_2O_3$ nanoparticles | CR | 254 | [54] |
| Mg–Fe–$CO_3$-LDH | CR | 105 | [55] |
| plate-like Mg-Al–LDH | CR | 143.3 | [56] |
| Ni/Mg/Al layered double oxides | CR | 1250 | [57] |

**Figure captions**

**Fig 1.** Schematic illustration of the synthesis and calcination of Ca-Al-LDHs and Ca-Al-LDOs.

**Fig 2.** XRD pattern of obtained Ca-Al-LDHs and Ca-Al-LDOs.

**Fig 3.** Different magnification SEM images of (a)-(c) Ca-Al-LDHs,(d)-(f) Ca-Al-LDOs.

**Fig 4.** TEM images Ca-Al-LDHs (a)-(b)and Ca-Al-LDOs (c)-(d);element mapping images of the Ca-Al-LDOs (e, f, g) and EDS pattern of Ca-Al-LDOs (h).

**Fig 5.** $N_2$ adsorption-desorption isotherms of as-obtained Ca-Al-LDHs (a) and Ca-Al-LDOs (b); the corresponding BJH desorption pore size distributions curve (inset).

**Fig 6.** FT-IR spectra of the Ca-Al-LDHs and Ca-Al-LDOs.

**Fig 7.** XPS survey spectrum (a), high-resolution XPS spectra of Al 2p (b), Ca 2p (c), and O 1s (d) of the Ca-Al-LDOs sample.

**Fig 8.** Effect of contact time on the adsorption capacity of CR on the Ca-Al-LDHs and Ca-Al-LDOs samples (adsorbent dose = 200 $mg \cdot L^{-1}$; CR concentration = 100 $mg \cdot L^{-1}$).

**Fig 9.** The pseudo-second-order kinetic plots of CR adsorption on Ca-Al-LDHs (a) and Ca-Al-LDOs (b). The inserted curve is the second step of pseudo-second-order kinetic plots on Ca-Al-LDOs

**Fig 10.** Adsorption isotherms of CR on the Ca-Al-LDHs and Ca-Al-LDOs samples at room temperature (adsorbent dose = 200 mg/L)

**Fig 11.** The recyclability of the Ca-Al-LDOs for the adsorption of CR.

**Fig 12.** The FT-IR spectra of Ca-Al-LDHs and Ca-Al-LDOs before and after CR adsorption and CR at 450–4000 $cm^{-1}$(a). The XRD patterns of Ca-Al-LDHs and Ca-Al-LDOs before and after CR adsorption (b).

**Fig 1.**

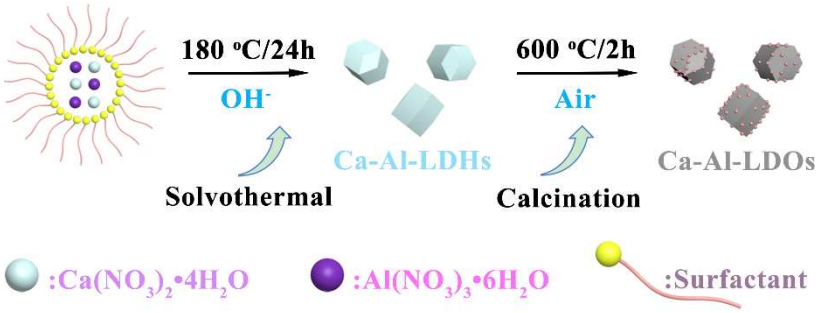

**Fig 2.**

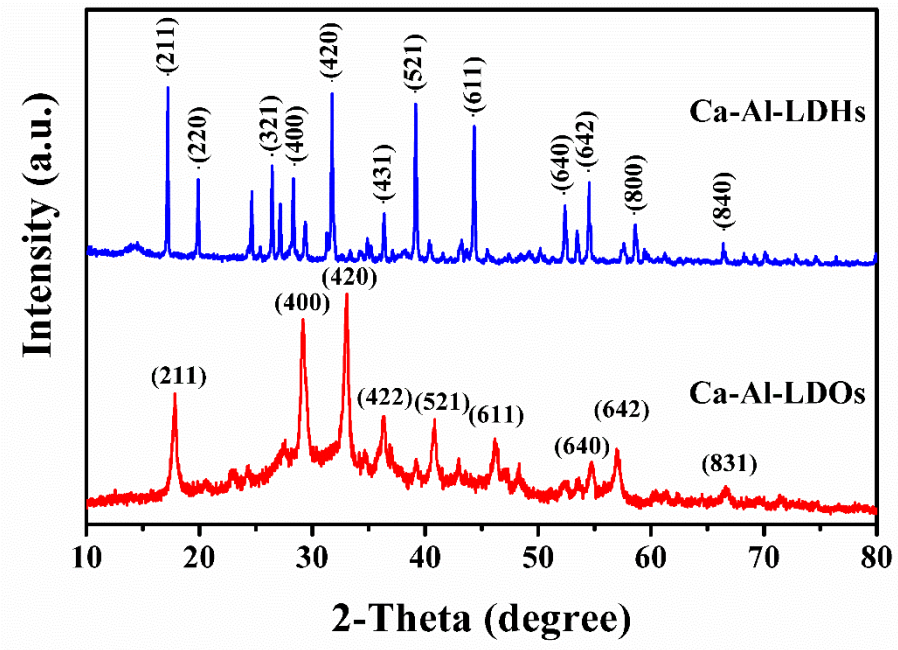

**Fig 3.**

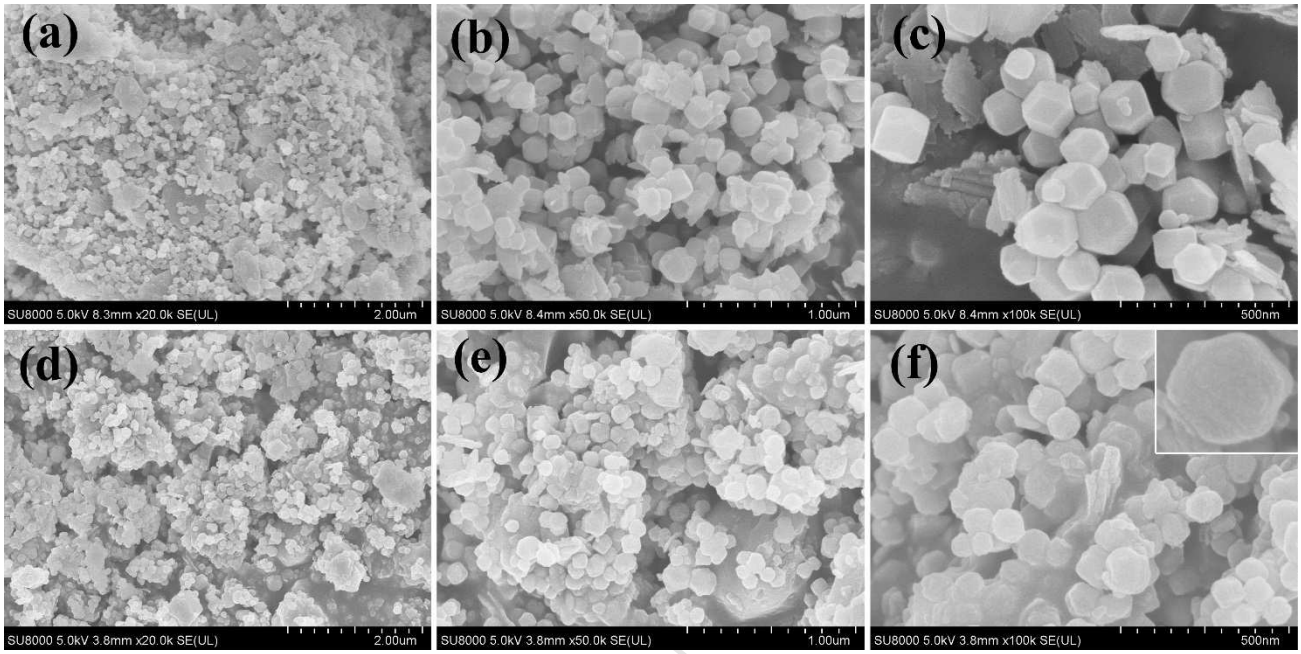

**Fig 4.**

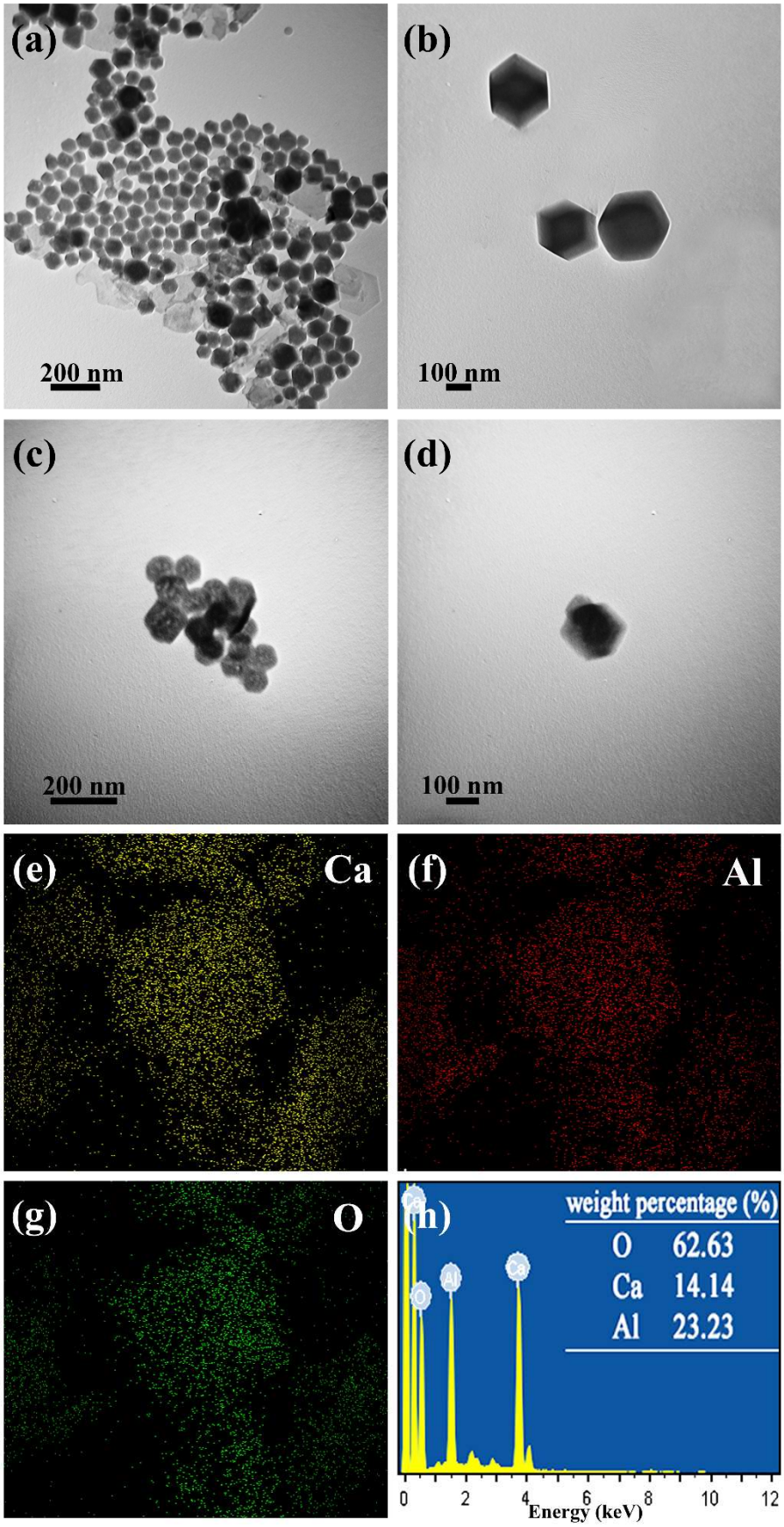
(a)
200 nm
(b)
100 nm
(c)
200 nm
(d)
100 nm
(e)
Ca
(f)
Al
(g)
O
(h)
weight percentage (%)
O 62.63
Ca 14.14
Al 23.23
0 2 4 6 8 10 12
Energy (keV)

**Fig 5.**

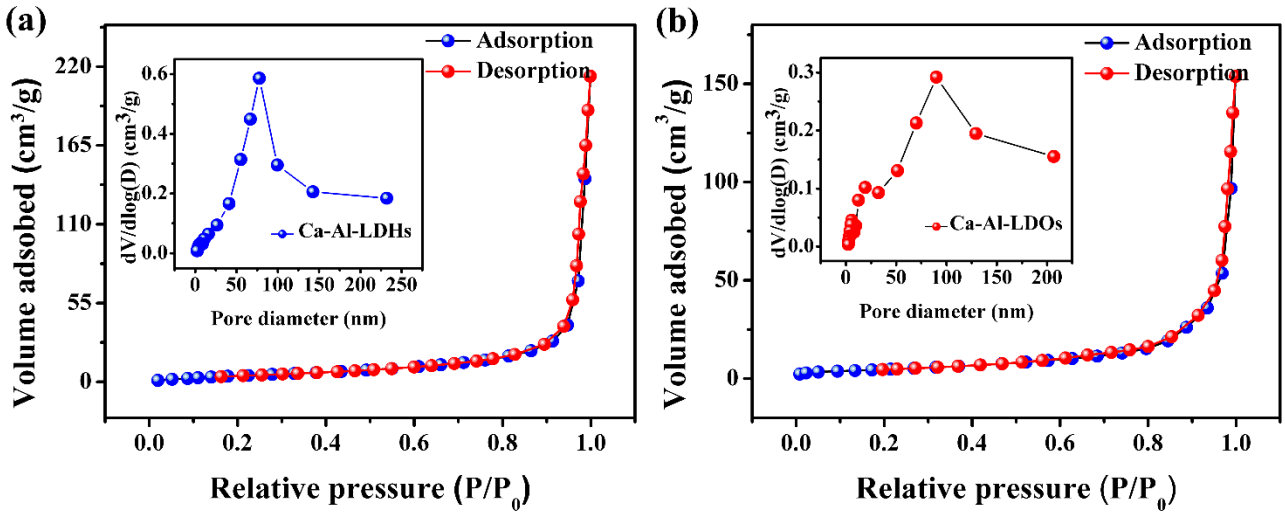

**Fig 6.**

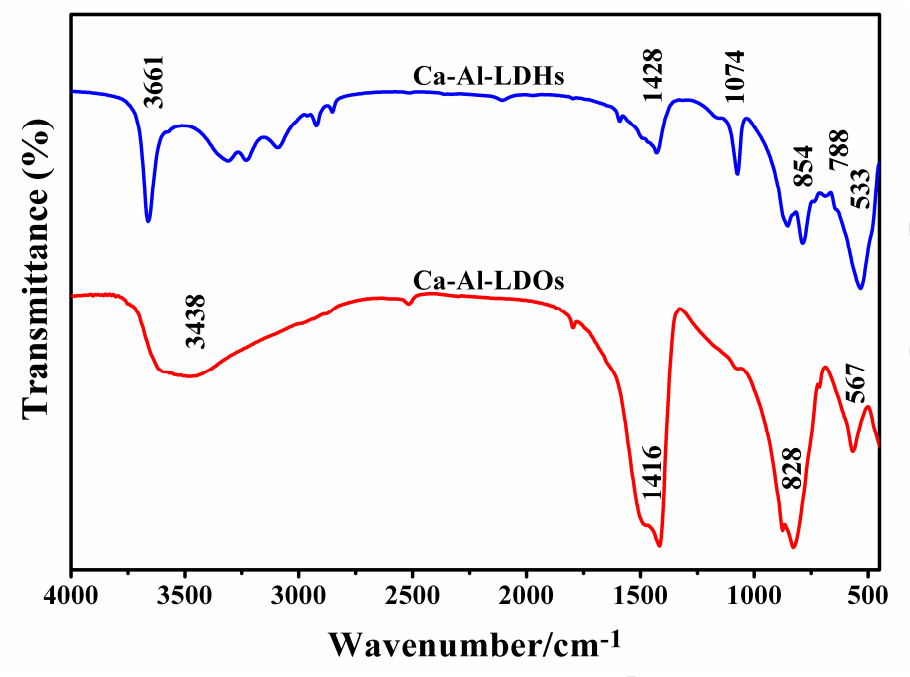

**Fig 7.**

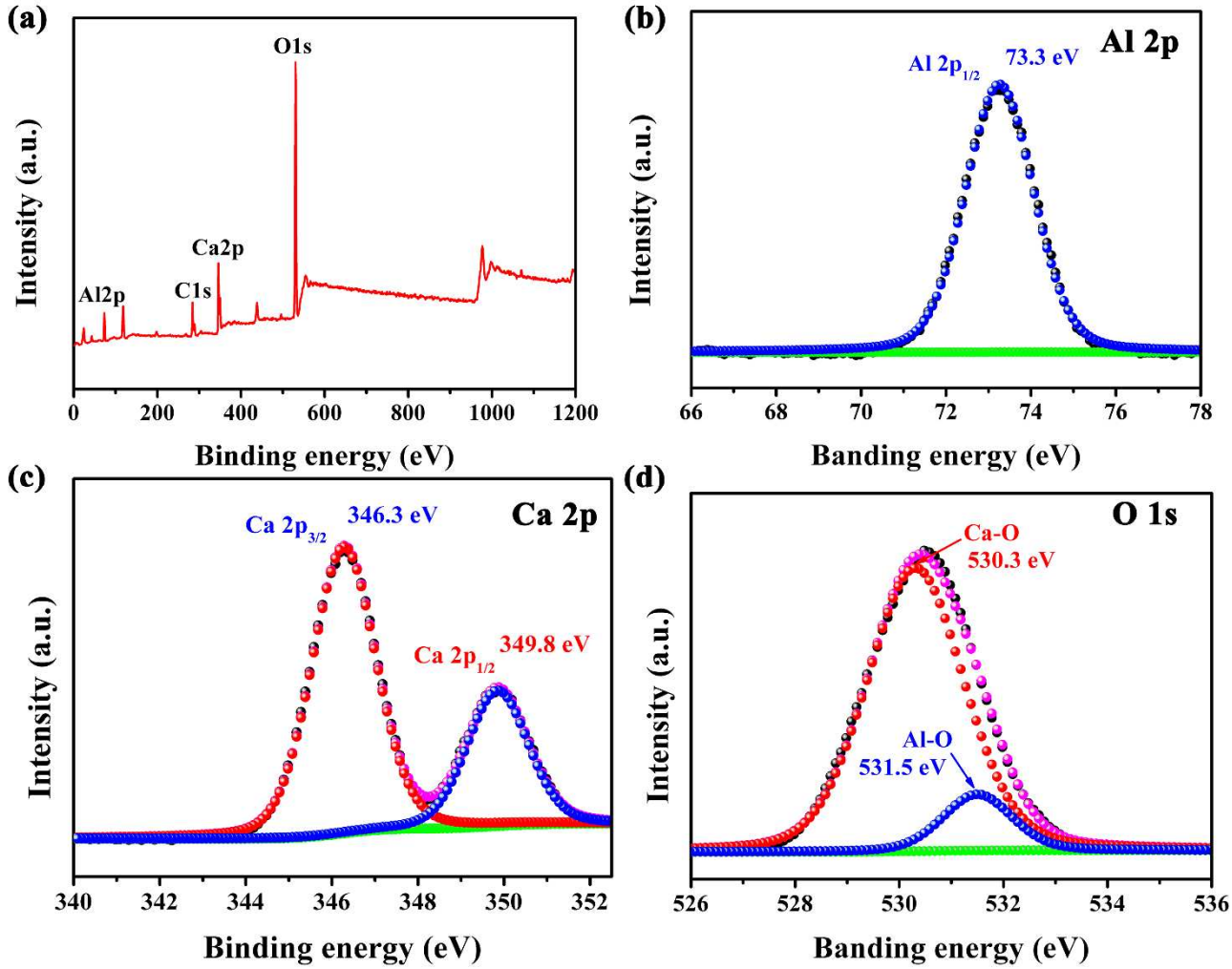

**Fig 8.**

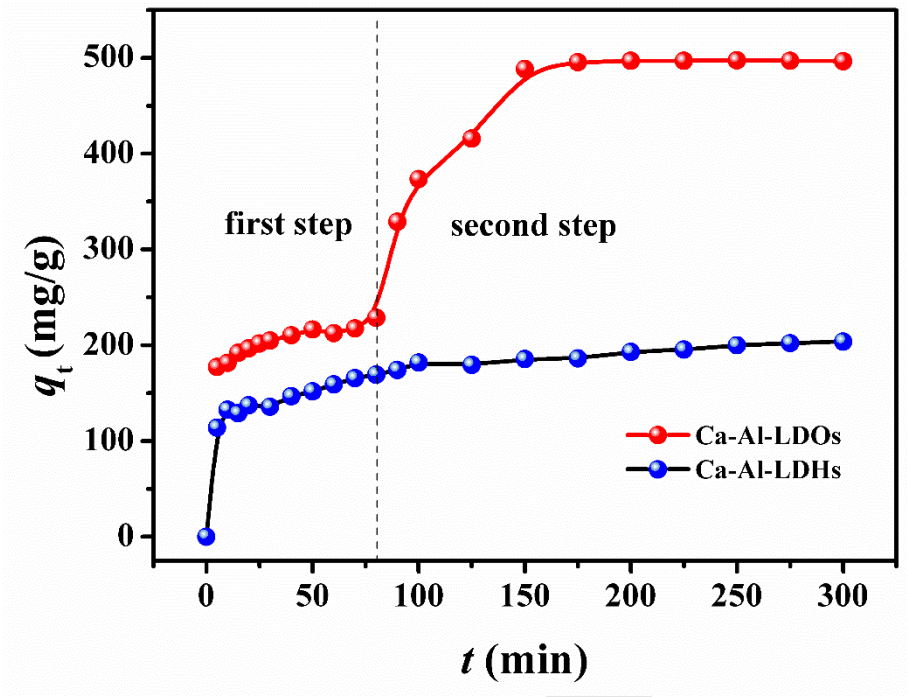

**Fig 9.**

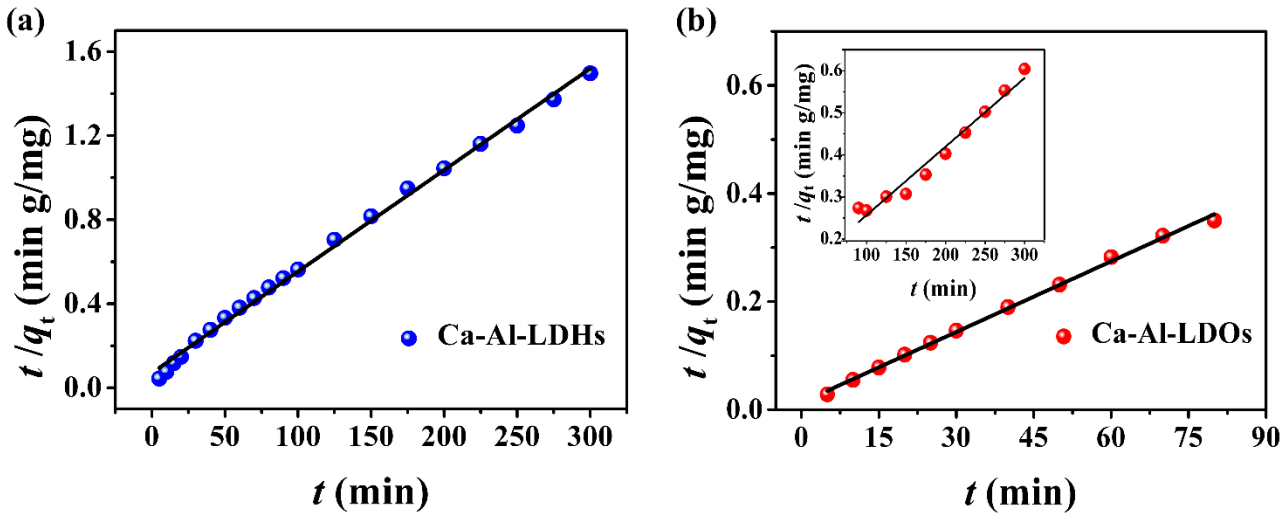

**Fig 10.**

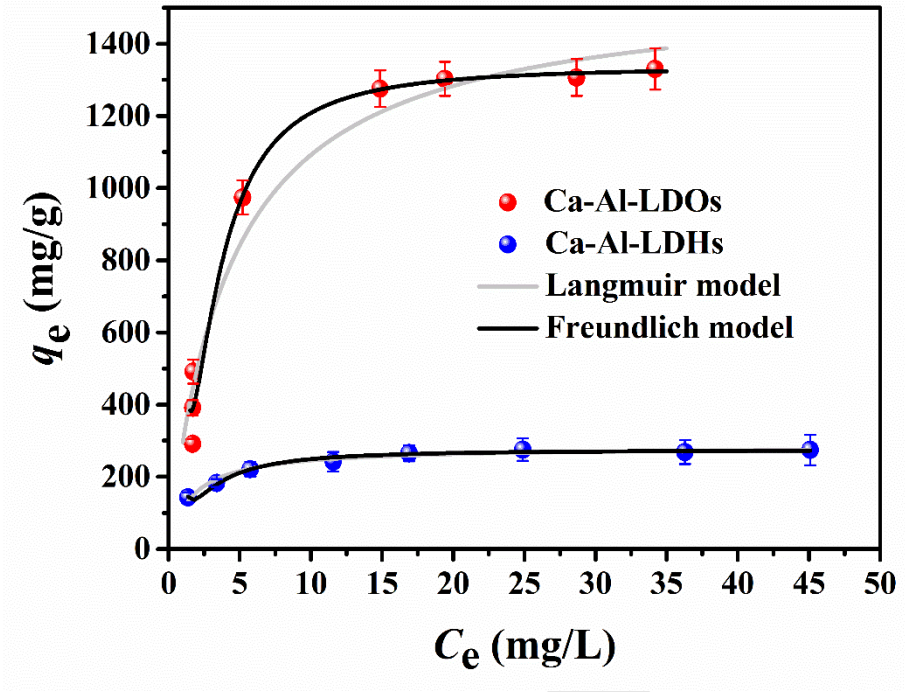

**Fig 11.**

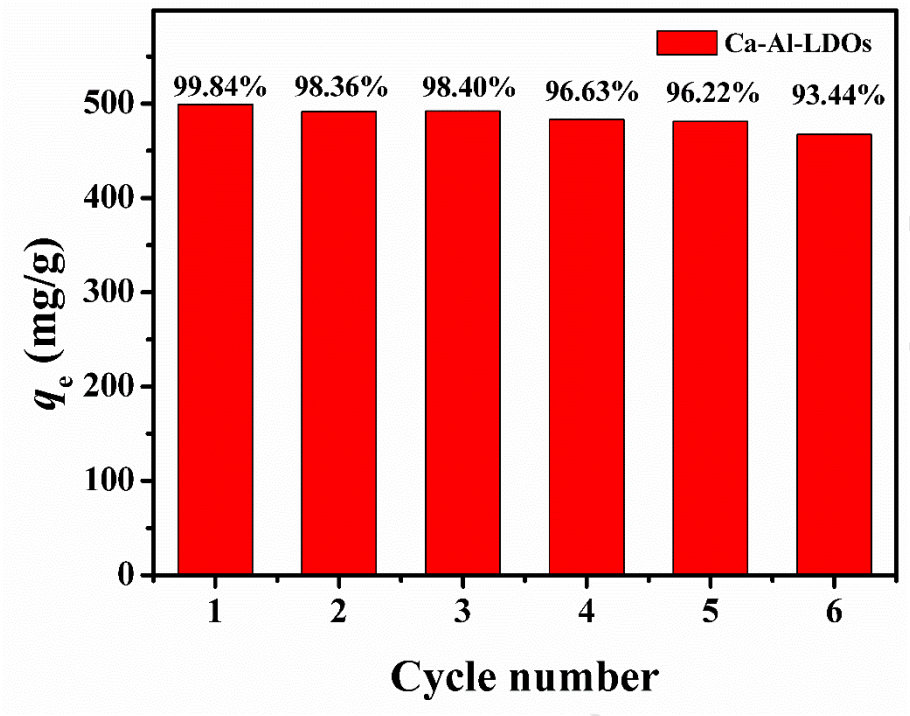

**Fig 12.**

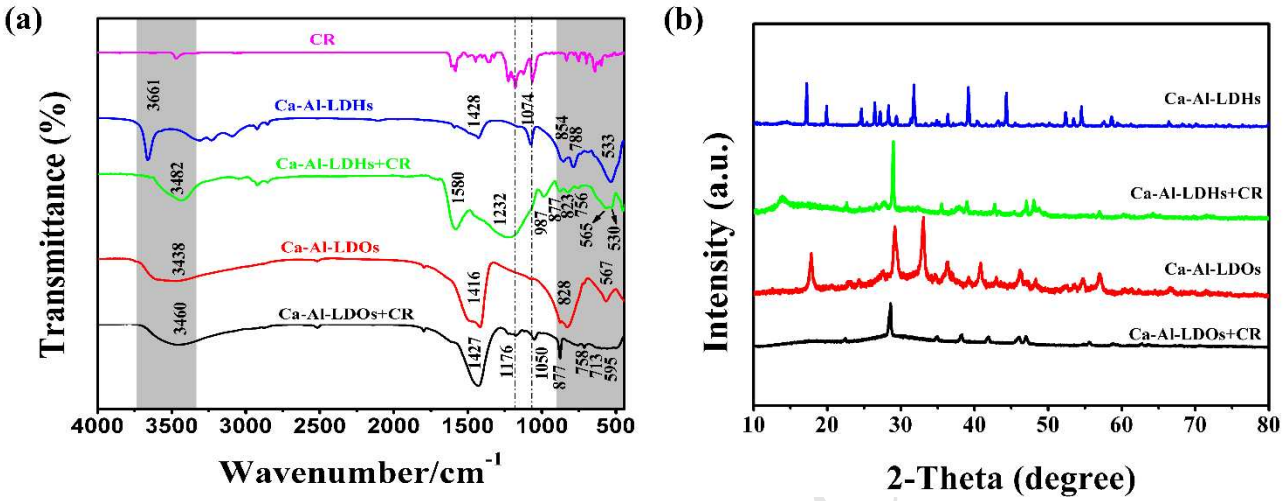

**Highlights:**

Ca-Al-LDHs were synthesized via a two-phase solvothermal method.

Ca-Al-LDHs and Ca-Al-LDOs with rhombic dodecahedral morphology.

The Ca-Al-LDOs has the maximum adsorption capacity of 1536.1 $mg \cdot g^{-1}$.